Journal of Industry, Engineering and Innovation, Vol. 1 No. 1 (2019) p. 1-10

JIEI

FAZ Publishing

Journal of Industry, Engineering and Innovation

Journal homepage : www.fazpublishing.com/jiei

e-ISSN : 2672-7382

Aerodynamic Analysis on the Effects of Different Type of Train's Nose Design using Ansys Software

Ahmad Nazirul Nazri[1], Izuan Amin Ishak[1], Nofrizalidris Darlis[1], Zuliazura Mohd Salleh[1], Shaiful Fadzil Zainal Abidin[1], Syabillah Sulaiman[1], Amir Khalid[1]

[1]Automotive and Combustion Synergies Technology Group, Faculty of Engineering Technology, University Tun Hussein Onn Malaysia (UTHM), Hub Pendidikan Pagoh, KM 1, Jalan Panchor, 84600 Pagoh, Johor, MALAYSIA

Email: ahmadnazirul11@yahoo.com

Received 00 Month 2000;
Accepted 01 Month 2000;
Available online 02 Month 2000

Abstract: The rapid development in engineering technology for train industry has allowed for the train to travel at higher speed. Train system provides large advantages to the users and the surrounding. There is a number of advantages of trains in terms of delivery as well as economic and environmental aspects. For this study, numerical techniques were adopted to study the aerodynamic analysis on different types of train nose design. The purpose of this study is to design different type of train's nose shape and compare the parameters of each design in term of aerodynamic drag, velocity streamline and pressure contour. This study will utilize the ANSYS Fluent software which is a CFD software. The behavior of fluid flow around the train is resolved by utilizing the Reynolds-averaged Navier Stokes (RANS) equations combined with the $Realizable\ k-\varepsilon^{a}$ equation model. The Reynolds number used is based on the height of the train and the freestream velocity was 3.7×10^5. In the result, it was found that the pressure coefficient and the drag coefficient is different between all models. The flow structure on the train model produce various pattern once the flow hit the frontal area of the train's nose. The fluid flow behavior around the train model was found to produce vortex. However, model with aerodynamic nose shape acquire less drag value, hence improve the efficiency of the train. Hence, Model 4 is the overall best model.

Keywords: Keywords: CFD, ANSYS Fluent, Drag Coefficient, Vortex, Simplified Train Model

1.0 Introduction

As the world's technology is improving, the train technological system also getting better day by day. There is a number of advantages of trains in terms of delivery as well as economic and environmental aspects. In term of economic, we all know that train system provides an affordable ticket price for the customers. In Malaysia, the train system is well known for its affordable ticket price compare to other public transport like buses and taxis. In term of environmental aspect, train system helps to save our climate since the current train's system only use electricity to move and does not produce a waste product from the engine. By using trains, air pollution in which is produces from the vehicle such as CO, NOX, and others can be reducing. The less the vehicle on the road, the healthier our environment will be [1].

History records that for train operation accidents can occurred due to controllable mechanical problems as well as uncontrollable natural phenomena [2]. The controllable mechanical problems can happen due to part failure, maintenance problem, and service mistake while on the other hand, some of the uncontrollable natural phenomena like strong wind, crosswind and wind gust. Hence, it is a must for the safety aspects of the train operation to be studied more implicitly specially to provide to the demand of the faster-moving train vehicle. The main objective of this project is to study the effect of different train's nose on the aerodynamic phenomena and to stimulate the various shape of train nose design using CFD engineering software (ANSYS Fluent).

2.0Literature Review

2.1Reynolds Number

The Reynolds number is used to study fluids as they flow. Reynolds number can be expressed as:

$$Re = \frac{\rho \times V \times L}{\mu}$$

where ρ is density of the fluid, V is velocity of the fluid, L is the characteristic linear dimension or length of fluid and μ is dynamic viscosity of fluid [4].

**Corresponding author: author@organization.edu.co*

Based on Copley [5], findings stated that flow field around the train is laminar and always attached to the surface of the train in the case of very low Reynolds number, Re. However, at large enough Reynolds number and for the case of flow over a train vehicle, there are a number of researchers who claimed that the influence of Reynolds number on aerodynamic coefficients is very little. Hemida & Krajnovic [6] also mentioned that for the range of $3.0 < Re < 3.7 \times 10^5$, the flow is fully turbulent and the aerodynamic coefficients are deduced to be independent of the Re since the drag crisis occurs at a much lower Re. Lastly, Mohebbi & Rezvani [7] which performed numerical analysis of the aerodynamic performance of a regional passenger train under crosswind conditions also realized that the aerodynamic coefficients can be considered constant for the entire range of the Reynolds number ($7.0 < Re < 25.0 \times 10^5$).

2.2 Aerodynamic on Train

Based on study of aerodynamics of high-speed trains by Schetz [8], there is a slight difference in drag produced by a large variety of slender shapes if the sharp edges are avoided. The effects of the nose shape on the overall drag of a train occurs due to the contribution of the total drag i.e. pressure drag and skin drag. The drag force only affected when the turbulent boundary was considered. Based on Copley [9], the shape of the train nose has only a slight influence on the pressure jump of the initial compression wave but clearly minimizes the maximum of the pressure gradient. An elliptical shape makes the compression wave reach its peak more rapidly, while parabola and cone shapes delay the wave.

2.3 Generic Train Model

In the context of the train's geometry, based on past investigation, some have considered much more advanced geometries by considering additional structures like a front spoiler, bogies, and mechanical device, while others define their structures in an exceedingly more simplified way. Based on Chiu and Squire [10], several complexities were concerned within the flow over a real train. Hence, it is impossible to generate complete modelling of these complexities. Furthermore, in an exceedingly recent study by Hemida and Krajnovic [11], train model used lacked underbody complexities and inter-carriage gaps between coaches. However, they managed to attain similar results with previous studies that used additional complex models. Liu *et al.* [12] conjointly chosen to implement far more simplified models of the trains by omitting the bogies and projecting equipment such because the pantograph.

2.4 Computational Fluid Dynamic

Computational Fluid Dynamics (CFD) is a branch of fluid mechanics that uses numerical methods and algorithms to solve and analyze problem that involves fluid flow. CFD modeling is based on fundamental governing equations of fluid dynamics like the conservation of mass, momentum, and energy. CFD helps to predict the fluid flow behavior based on the mathematical modeling using software tools. It is now widely used and is acceptable as a valid engineering tool in the industry [13].

The field of computational Fluid Dynamics became a commonly applied tool for generating solutions for fluid flows with or without solid interaction. In an exceedingly CFD analysis, the examination of fluid flow in accordance with its physical properties like velocity, pressure, temperature, density and viscosity is conducted. To virtually generate a solution for a natural phenomenon related to fluid flow, without compromise on accuracy, those properties need to be considered at the same time. In recent years, CFD modelling has come to be used more and more in the study of train aerodynamics and such techniques have a great deal to offer in terms of the detail that they can provide concerning the flow field around trains usually to a much higher resolution than is available from experimental data [14].

3.0 Methodology

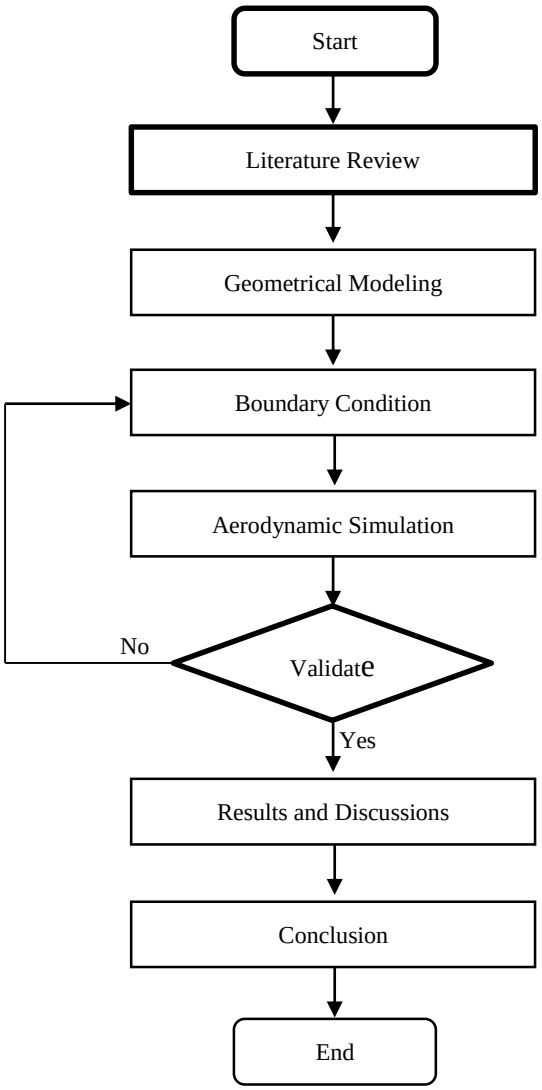

Figure 1: Flowchart for the simulation process.

3.1 Model Description

There are in total four model of different nose shape that were chosen in this study. As stated in the literature, there are some simplifications has been made for the sake of simplicity of this study. The train model is not including the window, boogies and door. The basic dimension of the train nose includes the length, width, height and fillet was obtained by comparing from the previous study. All the basic dimension of the train is shown in the Figure 2 below

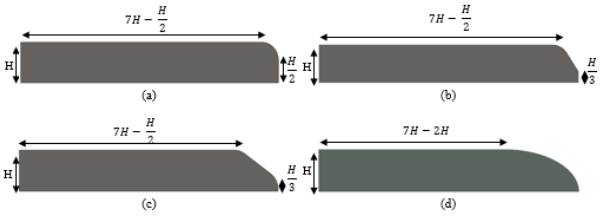

Figure 2: Geometry detail from side view (a) Model 1 (b) Model 2 (c) Model 3 and (d) Model 4

3.2 Boundary Condition

The main function of enclosure is to limit the simulation area so that the work become easier and more simple. The frontal surface of the enclosure will be the velocity inlet surface while the back part of the enclosure is the pressure outlet surface. Figure 3 below illustrate the boundary condition. While Figure 4 illustrate the enclosure setup. Actual simulation will have the train inside it, but for this explanation the train model will be neglected. General guidelines on the distances between the inlet and the vehicle and the vehicle and the outlet for the case study are based on the previous investigations which is Ishak *et al.* [15]. Based on former research on the simulation of flows around a generic train model, these specific lengths are found to be adequate to make sure the domain is at its optimum size and can also be considered large to ensure that the velocity and pressure fields are uniform at the inlet.

(a) ***Inlet:*** Uniform velocity, which represents the free stream velocity (U_∞) is applied in the *x*-direction.

(b) ***Ground plane:*** The boundary type of moving wall is applied with the velocity component in the *x*-direction equal to the inlet velocity (U_∞) in order to prevent the development of boundary layer on the ground plane. This is also to replicate the relative movement between the train and the ground.

(c) ***Outlet:*** The homogenous Neumann boundary condition is applied at the outlet, meaning that the pressure gradient is equal to zero. This allows the flow pass through the outlet without affecting the upstream flow, provided that the upstream distance to the vehicle's body is large enough.

(d) ***Lateral side and roof plane:*** The patch type boundary condition with a freestream value similar to the inlet is used.

(e) ***Train model surface:*** The no-slip condition is used.

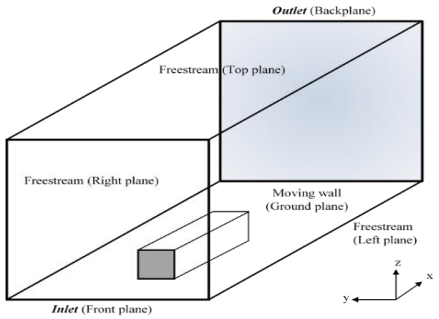

Figure 3: Enclosure setup for the boundary condition.

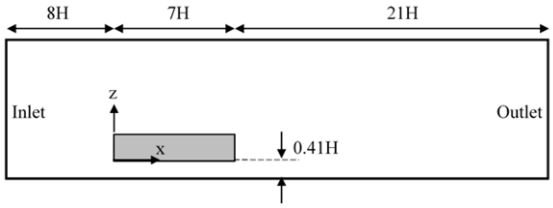

(a)

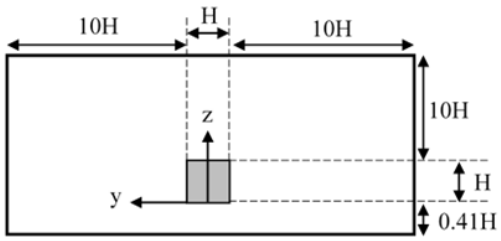

(b)

Figure 4: The enclosure dimension (not following the actual scale) of (a) Side view of computational domain and (b) Front view of the computational domain.

3.3 Geometry Meshing

The process of discretization model into number of elements is known as meshing [16]. It is the most important step in flow simulation analysis. The quality of mesh defines the accuracy of the results. The meshing of the model is done in ANSYS Fluent 19.1. Meshing will be applied on the enclosure and train body. The cells in the train and enclosure body are constructed using a meshing tool in the ANSYS Fluent software. For the meshing process, there only one grid resolution being used which is fine. Basically there are three grid resolution for meshing which are fine, medium and coarse.

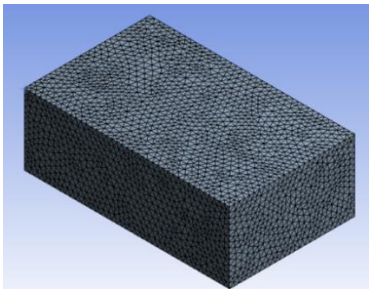

Figure 5: Meshing applied on enclosure Meshing is the most important part because more detailed mesh can produce more accurate result. Figure 5 above shows the meshing apply on the enclosure while Table 1 shows the meshing detail.

Table 1: Meshing detail

Detail	Model 1	Model 2	Model 3	Model 4
Relevance Centre	Fine	Fine	Fine	Fine
Smoothing	High	High	High	High
Cell Size, m	0.3	0.3	0.3	0.3
Total No. of Cells, N	477,106	464,113	478,384	488,677

3.4 Computational Methods

The numerical simulations in this study are implemented using the ANSYS Fluent software. Fluent software contains the broad, physical modelling capabilities needed to model flow, turbulence, heat transfer and reaction for industrial applications. Fluent also highly scalable to help solve complex, large-model computational fluid dynamics. The solution involving variety of cases required complex equation and calculation. Therefore, it is important to explain the numerical equations used in the research in the form of ANSYS Fluent representation as presented in this chapter.

3.4.1 Governing Equation

To solve the equations that describe the flow transport, transformation from partial differential equations to linearized algebraic equations is needed to be performed. This results in the following equations that are represented in nabla vector operator ∇:

$$\nabla . \boldsymbol{U} = 0 \tag{2}$$

$$\underbrace{\frac{\partial \boldsymbol{U}}{\partial t}}_{time} + \underbrace{\nabla . (\boldsymbol{UU})}_{divergence} - \underbrace{\nabla . (v \nabla \boldsymbol{U})}_{laplacian} = \underbrace{-\frac{1}{\rho} \nabla p}_{source} \tag{3}$$

where

$$\boldsymbol{U} = ui + vj + w \tag{4}$$

where p is the pressure, ρ is the fluid density, and v is the kinematic viscosity at an instantaneous time t and $\boldsymbol{U}$ is the local velocity in three spatial components (x, y and z).

The nabla operator is defined as:

$$\nabla = \frac{\partial}{\partial x_i} = \left(\frac{\partial}{\partial x_1}, \frac{\partial}{\partial x_2}, \frac{\partial}{\partial x_3}\right) \tag{5}$$

3.4.2 Discretization Method

Discretization method is an approach to solving complex mathematical functions by approximation. The method is associated with converting the continuous flow-related problems into discrete elements. This is then solved by approximating the transport equations into a discrete quantity using the discretization solvers. Solving a flow-related phenomenon using CFD is associated with discretization processes which is discretization of the governing equations [17].

There are few methods for the equation discretization including finite difference method (*fdm*), finite element method (*fem*), and finite volume method (*fvm*). Using *fvm*, the Partial Differential Equations (PDE) is transformed into a set of algebraic equations [18]. Similar to *fdm* and *fem*, quantities or variable are computed at discrete points or cells on a discretized geometry. A "finite volume" refers to a small volume surrounding each node point on a mesh.

Figure 6 shows a small fluid element of volume $V_p = dx \times dy \times dz$ with a center point **P** defined in the Cartesian coordinate system. This is an arbitrary control volume that is fixed in time and space, where the physical principles follow the preservation of both the conservation of mass and the conservation of linear momentum.

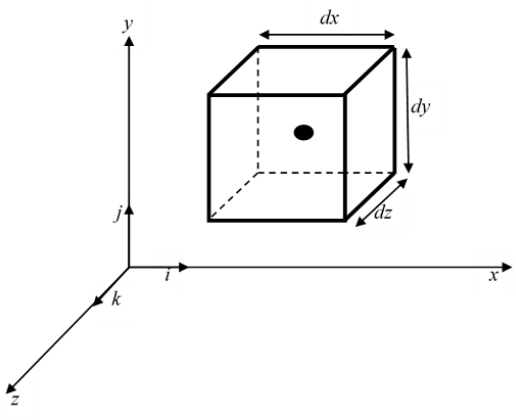

Figure 6: Control volume fluid.

The standard form of the transport equation for a scalar property ∅ is:

$$\underbrace{\frac{\partial \emptyset}{\partial t}}_{temporal\ derivative} + \underbrace{\nabla . (\boldsymbol{U}\emptyset)}_{convection\ term} - \underbrace{\nabla . (\Gamma_\emptyset \nabla \emptyset)}_{difussion\ term} = \underbrace{S_\emptyset(\emptyset)}_{source\ term} \tag{6}$$

Here, ∅ is the transport scalar like velocity, mass or sub-grid scale turbulent energy, Γ describes the diffusivity coefficient and S includes all source terms. Hence, for a control volume V_p at a time step ranging from t to $t + \Delta t$, the integral of a general transport equation for scalar quantities is written as follows:

$$\int_t^{t+\Delta t} \left[\underbrace{\frac{\partial}{\partial t} \int_{V_p} \emptyset dV}_{time} + \underbrace{\int_{V_p} \nabla . (U\emptyset) dV}_{divergence} - \underbrace{\int_{V_p} \nabla . (\Gamma_\emptyset \nabla \emptyset) dV}_{laplacian} \right] = \int_t^{t+\Delta t} \left(\underbrace{\int_{V_p} S_\emptyset(\emptyset) dV}_{source} \right) dt \tag{7}$$

Thus, solving the equation requires different discretization schemes such as time scheme, divergence scheme and laplacian scheme, to resolve each of the terms described in the equation above. As the diffusion term (laplacian) includes the second derivative (∇^2), the equation above can be regarded as a second-order equation. Based on Jasak [19], it is vital for the order of the discretization to be equal to or higher than the order of the discretized equation.

3.5 Validation of Study

The basic dimension of the train nose is including length, width, height and fillet was obtained by comparing from the previous study which are experimental by Sakuma *et al.* [20], numerical by Osth *et al.* [21] and Ishak *et al.* [22]. This dimension just average which is suitable for the simulation. The value of H is equal to 0.56 m. The simulation setup of current study with the previous study as in Table 2 below.

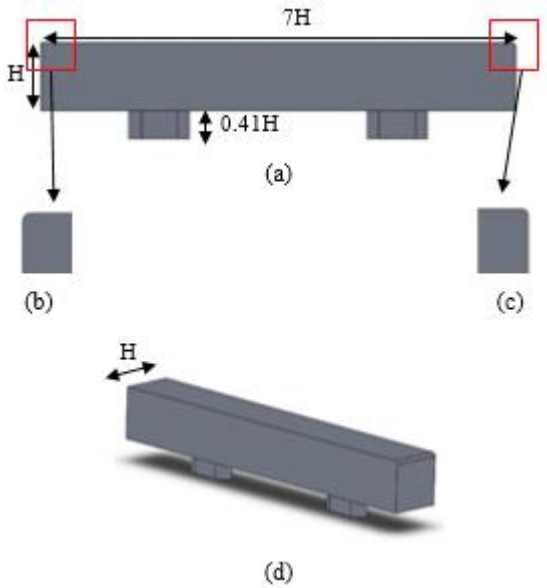

Figure 7: Geometry model for the train (a) Side view (b) and (c) Close up view of front and rear edges (d) Isometric view of the train model

The geometric configurations of the train model are explained below:

(a) The leading and top edges on the front are rounded using an elliptical profile with the major axis in the elliptical length of 0.07*H* and the minor axis length of 0.04*H* as can be seen in Figure 7(c).
(b) The side and top edges of the rear end of the vehicle are rounded with a circular radius of 0.107*H* as can be seen in Figure 7(b).
(c) Both front and rear bottom edges are not rounded and thus sharp.
(d) The length of the train is 7*H* while the width and height are both equal to *H* (*W* = *H* = 0.56 m).
(e) The model is placed on two egg-shaped supports and is lifted 0.41*H* above the ground in order to replicate the same condition as in the wind tunnel study by Sakuma *et al.* [20].

The model in Figure 7 above is only used for validation study only. As discussed on subtopic 3.1, that are the models designed for this study. The setup for this validation study as in Table 2 below. Since Sakuma *et al.* [20] doing experimental study, there is no simulation setup for that case. The simulation set-up discussing on the simulation model, the equations, the algorithm and the number of cells on meshing. On the other hand, Table 3 below shows the mean Cd results of validation study.

Table 2: Simulation set-up of the validation study.

Case	Osth *et al.* [21]	Izuan *et al.* [22]	Current Study
Simulation Model	PANS	URANS	RANS
Equations	Four model equations $(k-\varepsilon-\zeta-f)^a$	Two model equations • $STD\ k-\omega^2$ • $SST\ k-\omega^a$ • $STD\ k-\varepsilon^a$ • $Realizable\ k-\varepsilon^a$ One model equation • Spalart Allmaras	One model equations • $Realizable\ k-\varepsilon^a$ Wall Functions • $STD\ wall\ function$
Algorithm	SIMPLE	PISO	Coupled
No. of Cells	12 million	2 million	450,000 (average)

Table 3: Mean drag force coefficient for validation study

Case	Mean C_d
Experimental by Sakuma *et al.* [20]	0.86
Numerical by Osth *et al.* [21]	0.78
Numerical by Ishak *et al.* [22]	0.75
Current Study	0.60

As can be seen, the result obtained for mean C_d, is within the acceptable range. The result has proven that this study is on the right track in order to continue the study. However, the deviation of value might probably occur due to the much refine meshes used by previous researchers. The result differs also due to the different simulation setup and different equation model used.

4.0 Result and Discussion

4.1 Pressure Coefficient

Pressure coefficient is a dimensionless parameter which describes the relative pressures throughout a flow field in fluid dynamics. The pressure coefficient at a point near a body is independent of body size. An engineering model can be tested in wind tunnel or water tunnel, hence, pressure coefficients can be determined at critical locations around the model. So, in this research, the pressure coefficient is determined by the fluid flow on the train by running the simulation.

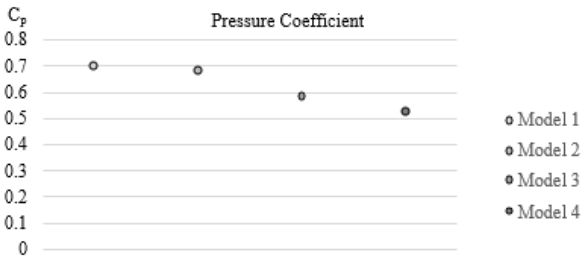

Figure 8: Comparison of pressure coefficient between different models.

Based on Figure 8, the trend of the graph decreasing between Model 1 and Model 4. Model 1 produce the highest pressure coefficient compare to the others. Model 4 has the lowest pressure coefficient among the others which is 0.52. Model 4 has the lowest pressure coefficient due to its aerodynamic shape. The elliptical shape helps the motion of the fluid to separate smoothly towards the surrounding and hence, reduce the drag forces. Compare to Model 3, it has the second lowest pressure coefficient which is 0.58. The different of Model 3 and Model 4 is the gradient of the front shape. Model 3 has sharp edge on the top part of the model while Model 4 does not have sharp edges. Thus, Model 3 produces vortex while Model 4 does not produce vortex on the top part. This vortex will be discussed further on subtopic 4.3. On the other hand, Model 3 has the highest value of pressure coefficient due to the sharp edges on the front surface of the train.

4.2 Drag Coefficient

In fluid dynamics, the drag coefficient is a dimensionless quantity that is used to quantify the drag or resistance of an object in a fluid environment such as air and water. It is used in the drag method where a lower drag coefficient means that there will be less aerodynamic or hydrodynamic drag on the object. A particular surface area is always correlated with the drag coefficient. In this research, the drag coefficient is calculated by the simulation after 200 iterations.

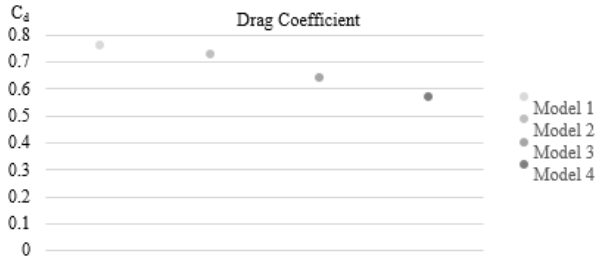

Figure 9: Comparison of drag coefficient between different models.

Based on Figure 9, the trend of the graph is decreasing from Model 1 to Model 4. This result is expected to be like this because of the shape of the model is designed to be from least aerodynamic shape to more aerodynamic shape. Hence, the simulation proves the hypothesis by producing this results. For this research, the positive drag value of four model contributed by the pressure due to combination of both skin frictions on the surface of the train and the pressure drag. Model 4 has the lowest drag force due to its elliptical shape and it has more aerodynamic design among the others. On the other hand, Model 1 has the highest drag force which is 0.76. Model 1 is designed to have a blunt nose surface which is the least aerodynamic design, thus producing high drag coefficient.

4.3 Streamline of Velocity Field on Mesh Body

In this study, the nature of flow field and its structure are visualized and examined by velocity streamlines. For this research, the velocity inlet has been set with 36 km/h for all model and the Reynolds number for this study is 3.7×10^5. Velocity used based on the same Reynolds number used by previous research which is Ishak *et al.* [22]. Figure 4.9 shows the velocity streamlines surrounding the train vehicle for the all models. The model is categorized by the shape of the train nose design which is blunt type and elliptical type. Model 1 and Model 2 can be categorized under blunt type, while Model 3 and Model 4 consist an elliptical nose design.

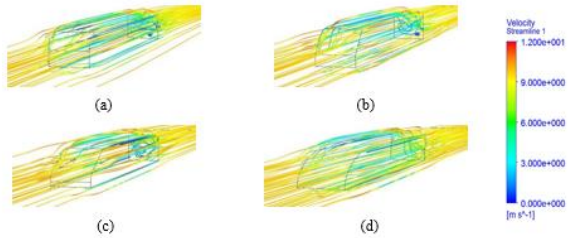

Figure 10: 3-D velocity streamline for different models (a) Model 1 (b) Model 2 (c) Model 3 and (d) Model 4

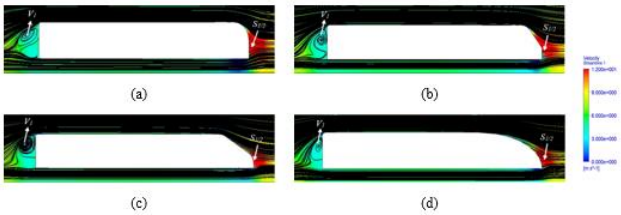

Figure 11: Velocity streamline from side view of different models (a) Model 1 (b) Model 2 (c) Model 3 and (d) Model 4

As shown in Figure 10, as the free stream flow approaches the nose surface, the flow particularly along the central axis is forced to move away from the body. A stagnation point appears at the central point of the model and can be clearly seen for all models in Figure 10. The pressure that hit the train surface create a drag. The different between Model 1 and Model 2 is the position of the stagnation point produced which is denoted as half saddle-point, $S_{1/2}$. The stagnation point of Model 1 produces right at the center of the surface, while stagnation point of Model 2 produces below from the center. After the separation of the stagnation point at both edges, the flow goes into various direction across the vehicle surface. Starting from the stagnation point, one part of the flow is oriented towards the bottom surface and the other part is oriented towards the roof surface of the train model. For Model 1 and Model 2, there is a well-defined vortex, V_1, produces behind the train when moving on to the downstream body. The bubbles produced when there is changes in the medium of the flow fluids.

In contrary, the flow structure is massively dissimilar in both sizes and shapes for Model 3 and Model 4 when the flow passes through. At the frontal region, the stagnation point can be visualized as the flow deteriorates instantly at the train's nose, but the location is slightly on the lower end area as denoted by the stagnation point in the same figure. The denotation of half saddle-point, $S_{1/2}$, also can be clearly seen. Refer to Figure 11(c) and Figure 11(d), there is differences in circularly flows vortex, V_1, produces behind the train of the elliptical design when moving on to the downstream body. Model 4 produces the smallest vortex compare to other models, while Model 3 produces the largest vortex at the back part. Model 4 has the lowest value of velocity produce on the top part. The flow does not separate after the stagnation point due to the no sharp edges on top of the train model. Hence, it creates different type of vortex on the downstream body.

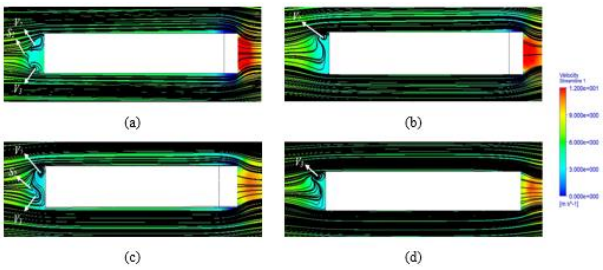

Figure 12: Velocity streamline from top view of the train (a) Model 1 (b) Model 2 (c) Model 3 and (d) Model 4

In general Figure 12, shows the streamlines from the horizontally symmetrical plane. The main features of the flow in this plane are two shear layers originating from the leading edges of the model and the reversed flow region downstream of the model. As the bifurcating streamlines of the incoming flow approaches the front surface of the model, a half saddle point, $S_{1/2}$ appears on the front surface as mentioned previously. When the flow goes into both side of the train, it produces a flow stream beside the train and low pressure region. The flow equally separate after hitting the nose area to both side of models.

From Figure 12(a), the separation occurs at both front side edges and it develops instantly as the flow moves past it. Both vortices (V_2 and V_3) that appear on the back edges of both sides are also found to be in much smaller in size which results in weaker pressure. Between the two vortices (V_2 and V_3), there is a saddle point, S_2. The illustration in Figure 12(b) clearly displays the lines of the separated flow region that originates from the side leading edges and sheds away downstream.

On the other hands, Model 2 does not produce the same fluid behavior as Model 1. On Figure 12(b), going downstream of the model, there is only one vortex (V_1) appear as the flow start to diverged. The vortex produces also smaller and thus producing low pressure region. For Model 3, the character of the vortex produces close to the Model 1 but different is size. For Model 4, the vortex produces on the back part of the train same as the Model 2. The different is in the size of the vortex and the speed of the flow. Model 4 produces high velocity vortex as the flow coming from the front. As mention previously, Model 4 does not create much separation as the flow hit the frontal region.

4.4 Pressure Contour

The result discussion continues with different presentation which is using pressure contour applied on the train. Due to the variations in the train design, the pressure exerts on the train's body will also behave differently. The objective of presenting the pressure contour is to visualize the pressure exerted on the train body through all sides and its relationship with the velocity streamline.

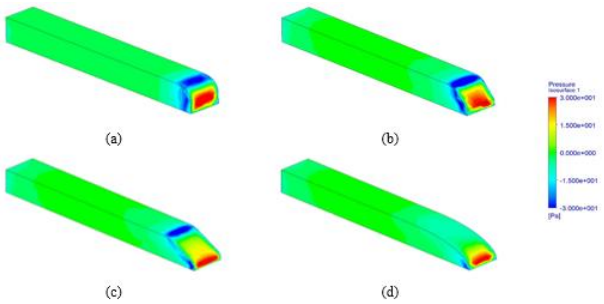

Figure 13: Isometric view of pressure contour (a) Model 1 (b) Model 2 (c) Model 3 and (d) Model 4

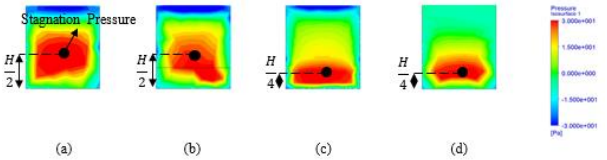

Figure 14: Front view of pressure contour (a) Model 1 (b) Model 2 (c) Model 3 and (d) Model 4

The front leading edge surface of the body gets hits by large pressure compare to the other surface. Refer to Figure 13, the pressure is uniformly exerted by the frontal surface of the train model. At this condition, as a result of flow separation at the front leading edge from top bottom and both side edges, a recirculation region forms producing vortices on the side and back of the trains. Hence, this result in low pressure regions on all surfaces near the leading edges. The size of low pressure region based on the size of vortices formed.

Refer to Model 1 (Figure 13(a)), the pressure exerts on the frontal area distributed equally and the flow separate equally to various side. The red region also known as the stagnation pressure and its appear at H/2 m. Hence, producing low pressure region occurs on the top and both side of the train. At the top part, the pressure exerts on the train lower (blue region) since there is flow separation. On the other hand, at the both side of the train nose also produce low pressure region. As discussed earlier (refer Figure 12), there is separation on both side of the train that make the flow increase and also producing vortices. For Model 2, the pressure exerts on the frontal leading surface hit at the center part exactly at H/2 m (refer Figure 14(b)). The pressure still exerts on the center part of the frontal area, but its gradually decrease in pressure as it goes upward. This is due to the frontal area of Model 2 consists of gradient surface and hence make the flow to go upward. At the top, the flow separate and producing vortex, hence, lowering the pressure on that area. The low pressure region continuous at both side follows the shape of the frontal area of the train.

In contrast for elliptical nose model which is Model 3 and Model 4, the stagnation pressure produce at lower area of the nose exactly at H/4 m (refer Figure 14(c) and Figure 14(d)). This is due to the flow that is hitting at the most frontal position of the train's nose located at the H/4 m. For Model 3, the pressure exerts on the frontal surface slowly faded when it goes upward. At the top part, Model 3 produce low pressure region since there is vortex produce. On the other hand, there is low pressure region on both side but much lower in magnitude compare to blunt nose design (Model 1 and Model 2). At the side part of the Model 3, there is low pressure contour produce from the center part going down to bottom area (refer Figure 14(c)). This is due to the separation at the

bottom area from the front is bigger compare to the center part. The flow that separate at the center part is lower compare to the bottom area. Model 4 does not produce vortices on top side because it considers as elliptical shape. This phenomenon occurs due to the no sharp edges at the top surface hence does not producing vortex and resulting normal pressure region. It is obvious that the pressure on the train's surface is different compared to that on the blunt nose shape which is due to the different geometry. After the stagnation point, the stream continuously flows without any separation, hence resulting no vortex produces at the top surface.

5.0 Conclusion

After conducting this study, the aerodynamic effects on different train's nose design has successfully achieved. The result obtained using CFD software is discussed. From the study, it is proved that pressure is inversely proportional with the velocity. As the velocity increase, the pressure on that area will decrease. The drag coefficient and pressure coefficient of four model were found to be different. Based on the results, Model 4 is the best train's nose design compare to other models. Model 4 produce the lowest drag coefficient and pressure coefficient. Due to its elliptical design, the flow separation produce after its encounter sharp edges is lower compare to the other models. Model 4 produce the smallest flow separation, hence resulting in low pressure drag. Meanwhile, the highest drag coefficient produces by Model 1. This happened because the nose shape design of Model 1 is blunter compare to other models. Consequently, Model 1 also produce the largest vortex comparing to the other models at the back part of the train. Along this study, there are few problems and limitations appear. The CFD software that been used are only for educational purpose only and not for research purpose. The problem is that it cannot load more than 520,000 number of cells from the meshing. The meshing cannot be further refine in order to get more accurate results. Thus, it has been deciding to not further refine the model. However, the software (ANSYS Fluent) still provide good results for the study.

References

[1] Rail Transportation. (2018). Retrieved from Enviro Literacy: https://enviroliteracy.org/environment-society/transportation/rail-transportation/

[2] Ministry of Transportation Malaysia. (2014). Retrieved from Statistic of Malaysia Transportation: https://www.jpj.gov.my

[3] Wikipedia Contributors (12 April 2019). Wikipedia the Free Encyclopedia. Retrieved from Aerodynamics: https://en.wikipedia.org/wiki/Aerodynamics

[4] N. Y. (2018). History Studies. *International Journal of History*, 241 - 264.

[5] T. W. Squire (1992). An experimental study of the flow over a train in a crosswind at large yaw angles. *J. Wind Eng. Ind. Aerodynamic*, 45(1), 47-74.

[6] H. Hemida and S. Krajnovic, (2009). Exploring Flow Structures Around a Simplified Ice2 Train Subjected to 30degress Side Wind using Les. *Engineering Application Computational. Fluid Mech*., 3(1), 28-41.

[7] M. Mohebbi and M. Rezvani (2013). Numerical analysis of aerodynamic performance of regional passenger train under crosswind conditions. *Int. J. Veh. Struct. Syst*, 5(2), 68-74.

[8] J. A. Schetz, (2001). Aerodynamics of High-Speed Trains. *Annu. Rev. Fluid Mech*, 33, 371-414.

[9] J. M. Copley, (1987). The Three-Dimensional Flow Around Railway Trains. *J. Wind Eng. Ind. Aerodynamic*, 26(1), 21-52.

[10] Baker, C. J. (1986). Train Aerodynamics Force and Moments from Moving Model Experiments. *Wind Engineering and Industrial Aerodynamics*, 24(3), 227 - 251.

[11] H. Hemida and S. Krajnovic (2008). Numerical Simulations of Flows Around Trains and Buses in Crosswinds. *17th AIAA Computational Dynamics*.

[12] Y. Liu, H. Hemida and Z. Liu, (2013). Large Eddy Simulation of the Flow Around a Train Passing a Stationary Freight Wagon. *Proc. Inst. Mech. Eng. Part F. J. Rail Rapid Transit*, 228(5), 1709-1718.

[13] Dynamics, C. F. (n.d.). Analysis of Fluid Flow for Objects. Retrieved from PES Performance: https://www.pes-performance.com/analysis-and-simulation/computational-fluid-dynamics/

[14] Computational Fluid Dynamics. (n.d.). Retrieved from What is CFD? https://www.simscale.com/docs/content/simwiki/cfd/whatiscfd.html

[15] I. A. Ishak, M. S. (2016). Numerical Simulation of Flow Around a Simplified High-Speed Train Model Using OpenFOAM. *IOP Conf. Ser. Mater. Sci. Eng*., 152, 3-14.

[16] ANSYS Fluent Software. (n.d.). Retrieved from CFD Simulation: https://www.ansys.com/products/fluids/ansys-fluent

[17] P. Wesseling (2001). Principle of Computational Fluid Dynamics. Springer-Verlag Berlin Heidelberg.

[18] CFD Online. (2012, August 28). Retrieved from Navier-Stokes Equation: https://www.cfd-online.com/Wiki/Navier-Stokes_equations

[19] H. Jasak (1996). Error Analysis and Estimation For The Finite Volume Method With Application of Fluid Flows. *Direct*, 394.

[20] S. Sakuma and Y. Ido (2009). Wind Tunnel Experiments On Reducing Seperated Flow Region Tunnel Around Front Ends of Vehicles On Meter-Gauge Railway Lines Vehicle Pressure Holf Tuft Position.

[21] J. Krajnovic (2012). Simulations of Flow Around a Simplified Train Model With a Drag Reducing using Partially Averaged Navier-Stokes. *Conference on Modelling Fluid*, 12.

[22] I. A. Ishak and M. S. (2016). Numerical Simulation of Flow Around a Simplified High-Speed Train

Model using OpenFOAM. *IOP Conf. Ser. Mater. Sci. Eng.*, 152, 80-85.